White Rose Research Online

eprints@whiterose.ac.uk
https://eprints.whiterose.ac.uk
Universities of Leeds, Sheffield and York

Deposited via The University of York.

White Rose Research Online URL for this paper:
https://eprints.whiterose.ac.uk/id/eprint/93314/

Version: Accepted Version

Article:
Flintoft, Ian David, Parker, Sarah, Bale, Simon Jonathan et al. (2016) Measured average absorption cross-sections of printed circuit boards from 2 to 20 GHz. IEEE Transactions on Electromagnetic Compatibility. pp. 553-560. ISSN: 0018-9375

https://doi.org/10.1109/TEMC.2016.2515658

Reuse
Items deposited in White Rose Research Online are protected by copyright, with all rights reserved unless indicated otherwise. They may be downloaded and/or printed for private study, or other acts as permitted by national copyright laws. The publisher or other rights holders may allow further reproduction and re-use of the full text version. This is indicated by the licence information on the White Rose Research Online record for the item.

Takedown
If you consider content in White Rose Research Online to be in breach of UK law, please notify us by emailing eprints@whiterose.ac.uk including the URL of the record and the reason for the withdrawal request.

UNIVERSITY OF LEEDS
University of Sheffield
UNIVERSITY of York

Author post-print

Measured Average Absorption Cross-Sections of Printed Circuit Boards from 2 to 20 GHz

Ian D. Flintoft, Sarah L. Parker, Simon J. Bale, Andy C. Marvin, John F. Dawson and Martin P. Robinson

Department of Electronics, University of York, Heslington, York YO10 5DD, UK

Published in IEEE Transaction on Electromagnetic Compatibility, vol. 58, no. 2, pp. 553-560, Apr. 2016.

Accepted for publication 29/12/2015

DOI: 10.1109/TEMC.2016.2515658

URL: http://ieeexplore.ieee.org/xpl/articleDetails.jsp?arnumber=7386654

© 2016 IEEE. Personal use of this material is permitted. Permission from IEEE must be obtained for all other uses, in any current or future media, including reprinting/republishing this material for advertising or promotional purposes, creating new collective works, for resale or redistribution to servers or lists, or reuse of any copyrighted component of this work in other works.

Measured Average Absorption Cross-Sections of Printed Circuit Boards from 2 to 20 GHz

Ian D. Flintoft, *Senior Member, IEEE*, Sarah L. Parker, Simon J. Bale, *Member, IEEE*, Andy C. Marvin, *Fellow, IEEE*, John F. Dawson, *Member, IEEE* and Martin P. Robinson

***Abstract*—The contents of an equipment enclosure, particularly printed circuit boards (PCBs), affect the enclosure's shielding performance. At high frequencies this absorption can be quantified using the angle of arrival and polarization averaged absorption cross-section (ACS). However, there is no available data on the high-frequency absorption characteristics of modern PCBs. In this study we apply a reverberation chamber to the determination of the average ACS of a large number of printed circuit boards taken from contemporary information and communication technology (ICT) equipment to provide a unique and comprehensive data-set. The ACS was found to range from 4×10^{-4} –10^{-2} m^2 from 2-20 GHz and different classes of PCB could be identified according to their surface characteristics. The "shadowing effect" of densely packed PCBs was also quantified for a subset of the PCBs. It was found that the ACS of a PCB in the stack was reduced by 20 % - 40 % compared to its value when isolated. By way of a review of the general power balance analysis of an electrically large populated equipment enclosure in an external environment we show how the acquired data will be useful for future qualification methodologies for ICT enclosures and PCBs.**

***Index Terms*—shielding, printed circuit board, absorption cross-section, reverberation chamber, immunity, emissions, power balance**

I. Introduction

The ever increasing operating frequencies of information and communication technology (ICT) systems is driving the requirements on electromagnetic shielding enclosures for the associated equipment to higher frequencies. ICT equipment is often configured as densely packed arrays of printed circuit boards (PCBs) inside shielded rack units. The absorption of electromagnetic power in the PCBs makes an important contribution to the level and distribution of the electromagnetic fields inside the enclosure and therefore to the overall immunity and emissions of the equipment. In this paper we report the measured absorption characteristics of a large set of ICT PCBs in the frequency range 2 to 20 GHz in order to provide an informative data-set for use in high-frequency shielding assessment and future qualification methodologies for ICT enclosures and PCBs.

The effect of an enclosure's contents on its shielding effectiveness has been studied experimentally over a number of years. At low frequencies the damping of resonances using absorbing material has been used to reduce both emissions and susceptibility of equipment [1], [2]. Efforts have been made to explicitly account for the effect of enclosure contents in shielding effectiveness metrics and measurement methodologies [3], [4]. IEEE Standard 299.1 contains an informative annex describing how to utilize absorbing materials in equipment enclosures for the measurement of shielding properties [5]. More recently, work has progressed to the consideration of higher frequencies using statistical approaches, particularly with regard to the effect of enclosure wall losses on shielding performance [6], [7].

The earliest models of equipment enclosures ignored their contents and thus underestimated the power losses. PCBs were included in simulations of cabinets by Wallyn and De Zutter who modeled them as thin sheets of perfect electric conductor [8]. This has the desired effect of perturbing the internal resonances, but does not account for the damping. The first enclosure model to include the effect of PCB losses appears to be that of Thomas et al who simulated the PCB as a lossy dielectric slab [9]. This model has been included in the simulations of several other researchers [10], [11]. Further work on modeling the effect of an enclosure's content on its shielding characteristics has been reported, mostly considering frequencies up to a few gigahertz [12], [13].

At high frequencies the absorption characteristics of a PCB can be quantified using its plane-wave absorption cross-section (ACS) averaged over angles of arrival and polarizations of the incident plane-wave. Average ACS is defined as the ratio of the average power absorbed to the average power density of the illuminating field. Such an average ACS can be measured in a reverberation chamber (RC) [14], [15]. The average ACS obtained from such measurements can be used directly in a power balance (PWB) analysis of populated ICT enclosures in an external environment to provide an estimate of the level of shielding provided by the enclosure [16], [17]. Providing the enclosure is electrically large and the PCBs are located more than about a quarter of a wavelength away from the walls of the enclosure the general validation of the PWB approach provided by

Submitted for review 14th August 2015. This work was supported by Huawei Technologies Co. Ltd., Shenzhen, P. R. China under Contract YB2014090010.

I. D. Flintoft, S. L. Parker, S. J. Bale, A. C. Marvin, J. F. Dawson and M. P. Robinson are with the Department of Electronics, University of York, Heslington, York, YO10 5DD (e-mail: {ian.flintoft, slp504, simon.bale, andy.marvin, john.dawson, martin.robinson}@york.ac.uk).

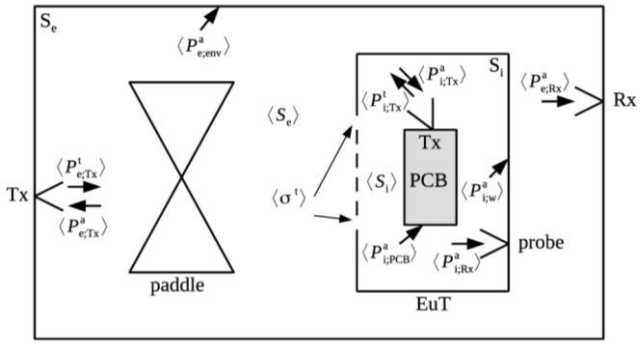

Fig. 1. Schematic illustration of an enclosure containing a PCB inside a reverberation chamber.

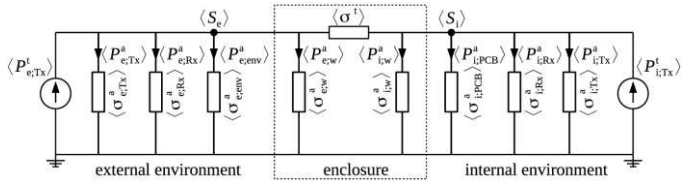

Fig. 2. Equivalent power balance circuit model for a populated enclosure in a reverberant environment.

[17-18] shows that it is an accurate method to determine the average internal fields. While the packing density in typical ICT enclosures is often so high that they cannot be regarded as ideal reverberation chambers the PWB approach can still be applied to provide a baseline reference for further experimental and numerical study. At very high frequencies some account of the "shadowing" effects of closely spaced PCBs can be incorporated into the analysis empirically.

In Section II we review the power balance analysis of a shielded enclosure with contents from both the immunity and emissions perspective to show how the ACS of PCBs directly contribute to the relevant metrics. A collection of 23 PCBs taken from two modern ICT enclosures is described and each PCB is classified in Section III. The methodology used to measure the ACS of each of these PCBs in a reverberation chamber over the band 2-20 GHz is described in Section IV. The results are presented in Section V and conclusions are drawn in Section VI.

II. Power Balance Analysis of Populated Enclosures

In this section we review the high frequency power balance (PWB) analysis of electromagnetic coupling into and out of an equipment enclosure which may contain lossy objects such as PCBs. The power balance method is described in detail by [18], [19]. The method is statistically based and applies quite generally, being a consequence of conservation of average electromagnetic power in a closed system. While typically applied to ideally reverberant systems, with electromagnetic field components whose real and imaginary parts are zero-mean Gaussian random variables, this is not a necessary requirement for the application of the technique; however, the approached is more powerful and predictive when applied to systems in which the underlying statistical distribution functions are known. Some of the equations in this section were obtained previously in specific contexts by other authors [6], [17]. Here we state the analysis in very general terms for both immunity and emissions perspectives explicitly including the internal contents of the enclosure.

A typical generic case is illustrated in Fig. 1. An equipment enclosure is located in a statistical environment S_e, for example, a reverberation chamber. The internal environment is denoted by S_i. For simplicity at this stage we will assume that the enclosure can be considered a single electrically large cavity with a set of contents – PCBs, looms, power supplies etc. The spacing between the contents and the walls of the enclosure is assumed to be at least a quarter of a wavelength so that the fields around them are well diffused. Both the external environment and enclosure are also assumed to contain two antennas, one transmitting (Tx) and one receiving (Rx). Fig. 2 shows the equivalent PWB circuit model for the system [19]. The average power densities in the external environment and enclosure are denoted by $\langle S_\mathrm{e}\rangle$ and $\langle S_\mathrm{i}\rangle$. Here $\langle\cdot\rangle$ denotes the average over an ensemble of systems, for example, in a reverberation chamber these could include the different positions of the mechanical tuner and different frequencies in a frequency tuning bandwidth. The total average transmission cross-section of the enclosure is

$$\langle\sigma^\mathrm{t}\rangle = \sum_j \langle\sigma_j^\mathrm{t}\rangle, \tag{1}$$

where $\langle\sigma_i^\mathrm{t}\rangle$ are the transmission cross-sections of all the individual apertures in the enclosure [18]. We assume that the walls are made of material with sufficiently large shielding effectiveness that any transmission through them can be neglected. The total average absorption cross-section of all the contents of the enclosure is similarly

$$\langle\sigma_\mathrm{i}^\mathrm{a}\rangle = \sum_j \langle\sigma_{\mathrm{i};j}^\mathrm{a}\rangle, \tag{2}$$

where $\langle\sigma_{\mathrm{i};j}^\mathrm{a}\rangle$ are the absorption cross-sections of each individual item (PCB, loom,…) within the enclosure. We can explicitly identify the absorption cross-sections of the internal side of the enclosure's walls, $\langle\sigma_{\mathrm{i;w}}^\mathrm{a}\rangle$, and the internal Tx and Rx antennas, $\langle\sigma_{\mathrm{i;Tx}}^\mathrm{a}\rangle$ and $\langle\sigma_{\mathrm{i;Rx}}^\mathrm{a}\rangle$, by writing

$$\langle\sigma_\mathrm{i}^\mathrm{a}\rangle = \langle\sigma_{\mathrm{i;w}}^\mathrm{a}\rangle + \langle\sigma_{\mathrm{i;PCB}}^\mathrm{a}\rangle + \langle\sigma_{\mathrm{i;Rx}}^\mathrm{a}\rangle + \langle\sigma_{\mathrm{i;Tx}}^\mathrm{a}\rangle, \tag{3}$$

where $\langle\sigma_{\mathrm{i;PCB}}^\mathrm{a}\rangle$ denotes the absorption by the remaining contents of the enclosure. Similarly for the external environment we write the total absorption cross-section as

$$\langle\sigma_\mathrm{e}^\mathrm{a}\rangle = \sum_j \langle\sigma_{\mathrm{e};j}^\mathrm{a}\rangle = \langle\sigma_{\mathrm{e;Tx}}^\mathrm{a}\rangle + \langle\sigma_{\mathrm{e;Rx}}^\mathrm{a}\rangle + \langle\sigma_{\mathrm{e;env}}^\mathrm{a}\rangle + \langle\sigma_{\mathrm{e;w}}^\mathrm{a}\rangle, \tag{4}$$

where $\langle\sigma_{\mathrm{e;w}}^\mathrm{a}\rangle$ is the ACS of the external side of the enclosure's walls, $\langle\sigma_{\mathrm{e;Tx}}^\mathrm{a}\rangle$ and $\langle\sigma_{\mathrm{e;Rx}}^\mathrm{a}\rangle$ are the ACSs of external transmitting and receiving antennas and $\langle\sigma_{\mathrm{e;env}}^\mathrm{a}\rangle$ is the ACS due to all other losses in the external environment.

The powers injected into the external and internal environments by the transmitting antennas are given by

$$\begin{aligned}\langle P_{\mathrm{e;Tx}}^\mathrm{t}\rangle &= \langle\eta_{\mathrm{e;Tx}}^\mathrm{T}\rangle\langle P_\mathrm{e}^\mathrm{f}\rangle \\ \langle P_{\mathrm{i;Tx}}^\mathrm{t}\rangle &= \langle\eta_{\mathrm{i;Tx}}^\mathrm{T}\rangle\langle P_\mathrm{i}^\mathrm{f}\rangle,\end{aligned} \tag{5}$$

where $P_{\mathrm{e/i}}^\mathrm{f}$ are the forward powers at the antenna ports and $\eta_{\mathrm{e/i;Tx}}^\mathrm{T}$ are the total efficiencies of the two transmitting

TABLE I
SHIELDING REGIMES. ACS AND $\langle SR_{\mathrm{IM}} \rangle$ ARE SPECIFIC TO THE IMMUNITY PERSPECTIVE AND TRP TO THE EMISSION PERSPECTIVE.

Shielding Regime	ACS (m^2)	$\langle SR_{\mathrm{IM}} \rangle$ (-)	TRP (W)
Perfect Shielding $\langle \sigma^{\mathrm{t}} \rangle \to 0$	$\langle \sigma^{\mathrm{T}}_{\mathrm{EUT}} \rangle \to \langle \sigma^{\mathrm{a}}_{\mathrm{e;w}} \rangle$	$\langle SR_{\mathrm{IM}} \rangle \to \infty$	$P^{\mathrm{TRP}} \to 0$
Good Shielding $\langle \sigma^{\mathrm{t}} \rangle \ll \langle \sigma^{\mathrm{a}}_{\mathrm{i}} \rangle$	$\langle \sigma^{\mathrm{T}}_{\mathrm{EUT}} \rangle \approx \langle \sigma^{\mathrm{a}}_{\mathrm{e;w}} \rangle + \langle \sigma^{\mathrm{t}} \rangle$	$\langle SR_{\mathrm{IM}} \rangle \to \frac{\langle \sigma^{\mathrm{a}}_{\mathrm{i}} \rangle}{\langle \sigma^{\mathrm{t}} \rangle} \gg 1$	$P^{\mathrm{TRP}} \ll P^{\mathrm{src}}$
Poor Shielding $\langle \sigma^{\mathrm{t}} \rangle \gg \langle \sigma^{\mathrm{a}}_{\mathrm{i}} \rangle$	$\langle \sigma^{\mathrm{T}}_{\mathrm{EUT}} \rangle \approx \langle \sigma^{\mathrm{a}}_{\mathrm{e;w}} \rangle + \langle \sigma^{\mathrm{a}}_{\mathrm{i}} \rangle$	$\langle SR_{\mathrm{IM}} \rangle \to 1$	$P^{\mathrm{TRP}} \approx P^{\mathrm{src}}$

antennas. The average powers absorbed by the receiving antennas are

$$\begin{aligned} \langle P^{\mathrm{a}}_{\mathrm{e;Rx}} \rangle &= \langle \sigma^{\mathrm{a}}_{\mathrm{e;Rx}} \rangle \langle S_{\mathrm{e}} \rangle \\ \langle P^{\mathrm{a}}_{\mathrm{i;Rx}} \rangle &= \langle \sigma^{\mathrm{a}}_{\mathrm{i;Rx}} \rangle \langle S_{\mathrm{i}} \rangle, \end{aligned} \tag{6}$$

where $\langle \sigma^{\mathrm{a}}_{\mathrm{e;Rx}} \rangle$ and $\langle \sigma^{\mathrm{a}}_{\mathrm{i;Rx}} \rangle$ are their respective average absorption cross-sections. Similar relations hold for the powers received by the transmitting antennas. The equivalent circuit can be solved for the power densities to give

$$\begin{bmatrix} \langle S_{\mathrm{e}} \rangle \\ \langle S_{\mathrm{i}} \rangle \end{bmatrix} = \frac{1}{\Delta} \begin{bmatrix} \langle \sigma^{\mathrm{a}}_{\mathrm{i}} \rangle + \langle \sigma^{\mathrm{t}} \rangle & \langle \sigma^{\mathrm{t}} \rangle \\ \langle \sigma^{\mathrm{t}} \rangle & \langle \sigma^{\mathrm{a}}_{\mathrm{e}} \rangle + \langle \sigma^{\mathrm{t}} \rangle \end{bmatrix} \begin{bmatrix} \langle P^{\mathrm{t}}_{\mathrm{e}} \rangle \\ \langle P^{\mathrm{t}}_{\mathrm{i}} \rangle \end{bmatrix}, \tag{7}$$

where the determinant is

$$\Delta = (\langle \sigma^{\mathrm{a}}_{\mathrm{e}} \rangle + \langle \sigma^{\mathrm{t}} \rangle)(\langle \sigma^{\mathrm{a}}_{\mathrm{i}} \rangle + \langle \sigma^{\mathrm{t}} \rangle) - (\langle \sigma^{\mathrm{t}} \rangle)^2. \tag{8}$$

A. *Immunity perspective –external source*

In the case where there is an external source only we find from (7) that

$$\langle SR_{\mathrm{IM}} \rangle \stackrel{\mathrm{def}}{=} \frac{\langle S_{\mathrm{e}} \rangle}{\langle S_{\mathrm{i}} \rangle} = \frac{\langle \sigma^{\mathrm{a}}_{\mathrm{i}} \rangle + \langle \sigma^{\mathrm{t}} \rangle}{\langle \sigma^{\mathrm{t}} \rangle} = 1 + \frac{\langle \sigma^{\mathrm{a}}_{\mathrm{i}} \rangle}{\langle \sigma^{\mathrm{t}} \rangle}, \tag{9}$$

which defines the average Shielding Ratio (SR) for the immunity perspective [4],[6],[18]. We avoid using the term "shielding effectiveness" since this is usually defined as a field ratio whereas the quantity above is a power density ratio. The overall loading effect of the equipment on the external environment can be found by determining the equivalent "admittance" of all the equipment related cross-sections to the right of the S_{e} node in the equivalent circuit. This gives the total absorption cross-section of the enclosure and its contents as

$$\langle \sigma^{\mathrm{T}}_{\mathrm{EUT}} \rangle = \langle \sigma^{\mathrm{a}}_{\mathrm{e;w}} \rangle + \frac{\langle \sigma^{\mathrm{a}}_{\mathrm{i}} \rangle}{1 + \frac{\langle \sigma^{\mathrm{a}}_{\mathrm{i}} \rangle}{\langle \sigma^{\mathrm{t}} \rangle}} = \langle \sigma^{\mathrm{a}}_{\mathrm{e;w}} \rangle + \frac{\langle \sigma^{\mathrm{a}}_{\mathrm{i}} \rangle}{\langle SR_{\mathrm{IM}} \rangle}. \tag{10}$$

The different regimes of the SR and equipment ACS are summarized in Table I. The table also shows the total radiated power (TRP) for a given internal source power (P^{src}) in the emission perspective to be introduced in Section II.B. As $\langle \sigma^{\mathrm{t}} \rangle \to 0$ the SR becomes large and the total ACS becomes bounded by the absorption in the external walls of the enclosure - the effect of the internal absorption within the enclosure is not apparent. When $\langle \sigma^{\mathrm{t}} \rangle \gg \langle \sigma^{\mathrm{a}}_{\mathrm{i}} \rangle$, $\langle SR_{\mathrm{IM}} \rangle \to 1$ and the total ACS is just the sum of the ACSs of the enclosure walls (internal and external) and contents. In this case the enclosure is not effective at reducing the internal power density inside the equipment and the shielding ratio approaches unity. We see from (10) that the apparent ACS of the contents seen from the external environment is their actual ACS scaled by $\langle SR_{\mathrm{IM}} \rangle$. Note also that in the good shielding regime the shielding ratio is directly proportional to $\langle \sigma^{\mathrm{a}}_{\mathrm{i}} \rangle$; for an empty enclosure $\langle SR_{\mathrm{IM}} \rangle$ is therefore dependent on the usually uncontrolled ACS of the internal walls of the enclosure as found by [6]. We see that both $\langle \sigma^{\mathrm{t}} \rangle$ and $\langle \sigma^{\mathrm{a}}_{\mathrm{i;w}} \rangle$ together characterise the intrinsic "shielding capability" of the enclosure, independently of the internal contents. However, knowledge of the SR for the empty enclosure itself does not allow the SR for a populated enclosure to be determined. Specifically the SR of the enclosure populated by contents with ACS $\langle \sigma^{\mathrm{a}}_{\mathrm{i;PCB}} \rangle$, denoted by $\langle SR^{\mathrm{populated}}_{\mathrm{IM}} \rangle$, is related to the SR of the empty enclosure, $\langle SR^{\mathrm{empty}}_{\mathrm{IM}} \rangle$, by

$$\langle SR^{\mathrm{populated}}_{\mathrm{IM}} \rangle = \langle SR^{\mathrm{empty}}_{\mathrm{IM}} \rangle + \frac{\langle \sigma^{\mathrm{a}}_{\mathrm{i;PCB}} \rangle}{\langle \sigma^{\mathrm{t}} \rangle}. \tag{11}$$

Since $\langle \sigma^{\mathrm{t}} \rangle$ is not determined by a measurement of $\langle SR^{\mathrm{empty}}_{\mathrm{IM}} \rangle$, the populated SR cannot be inferred, even if $\langle \sigma^{\mathrm{a}}_{\mathrm{i;PCB}} \rangle$ is known. $\langle \sigma^{\mathrm{t}} \rangle$ could in principle be determined by measuring the SR of an enclosure containing an object of known ACS.

B. *Emission perspective – internal source*

In the case where there is an internal source only, for example when considering the emissions of the equipment, we define the average shielding ratio by

$$\langle SR_{EM} \rangle \stackrel{\mathrm{def}}{=} \frac{\langle S_{\mathrm{i}} \rangle}{\langle S_{\mathrm{e}} \rangle} = \frac{\langle \sigma^{\mathrm{a}}_{\mathrm{e}} \rangle + \langle \sigma^{\mathrm{t}} \rangle}{\langle \sigma^{\mathrm{t}} \rangle} = 1 + \frac{\langle \sigma^{\mathrm{a}}_{\mathrm{e}} \rangle}{\langle \sigma^{\mathrm{t}} \rangle}. \tag{12}$$

This definition of average shielding ratio is not reciprocal with the immunity case:

$$\langle SR_{EM} \rangle \neq \langle SR_{IM} \rangle. \tag{13}$$

From (7) the average total radiated power (TRP) of a source located in the external environment, in the presence of the enclosure, is related to the external power density by

$$P^{\mathrm{TRP}} = \frac{\Delta}{\langle \sigma^{\mathrm{a}}_{\mathrm{i}} \rangle + \langle \sigma^{\mathrm{t}} \rangle} \langle S_{\mathrm{e}} \rangle. \tag{14}$$

Using (7) again the TRP (into the external environment) of an enclosure that contains an internal source radiating power P^{src} (into the internal environment) is thus

$$P^{\mathrm{TRP}} = \frac{\Delta}{\langle \sigma^{\mathrm{a}}_{\mathrm{i}} \rangle + \langle \sigma^{\mathrm{t}} \rangle} \frac{\langle \sigma^{\mathrm{t}} \rangle}{\Delta} P^{\mathrm{src}} = \frac{P^{\mathrm{src}}}{\langle SR_{\mathrm{IM}} \rangle}, \tag{15}$$

showing that the TRP of the EUT is the total power emitted into the internal environment, suppressed by the *immunity* shielding ratio. Since $\langle SR_{IM} \rangle$ depends on the ACS of the enclosure contents the total emissions are reduced by increasing the loading of the enclosure as shown by [7].

The power balance approach does not directly provide any information about the radiation pattern of the enclosure. At high frequencies the far-field radiation pattern can be highly directive due to the large phase variations across all the apertures in the enclosure [20]. The near-field emissions likewise vary extremely rapidly both spatially and with frequency [21].

C. Contribution of PCBs to the internal environment

The above analysis makes clear that the energy density inside the enclosure depends not only on $\langle\sigma^{\mathrm{t}}\rangle$, but also on the contents. We expect that in densely populated enclosures the losses in the contents will dominate the wall losses, $\langle\sigma^{\mathrm{a}}_{\mathrm{i;PCB}}\rangle \gg \langle\sigma^{\mathrm{a}}_{\mathrm{i;w}}\rangle$, and therefore the ACS of the contents has a key role in determining the immunity of the equipment. The immunity of a PCB inside an enclosure to external interference power is ultimately determined by the energy coupled to active devices on the PCB – i.e. absorbed power in devices. This in turn depends on the effective receiving aperture of each device port on the PCB and the power density in the enclosure. The absorption cross-section of the PCBs can, formally at least, be split into two components

$$\langle\sigma^{\mathrm{a}}_{\mathrm{i;PCB}}\rangle = \langle\sigma^{\mathrm{a}}_{\mathrm{i;passive}}\rangle + \langle\sigma^{\mathrm{a}}_{\mathrm{i;circuit}}\rangle, \tag{16}$$

where $\langle\sigma^{\mathrm{a}}_{\mathrm{i;passive}}\rangle$ corresponds to power absorbed in the passive structural components of the contents such as packaging, PCB substrates and cable dielectrics while $\langle\sigma^{\mathrm{a}}_{\mathrm{i;circuit}}\rangle$ is the component that is absorbed in the loads of the PCBs' circuits. Again rather formally we can write this component as

$$\langle\sigma^{\mathrm{a}}_{\mathrm{i;circuit}}\rangle = \sum_j \langle\sigma^{\mathrm{a}}_{\mathrm{i};j}\rangle, \tag{17}$$

where $\langle\sigma^{\mathrm{a}}_{\mathrm{i};j}\rangle$ are the absorption cross-sections into the loads of the PCBs' ports. The power coupled into the active devices on a PCB, and therefore its susceptibility, can be reduced by two methods:

1. By reducing the effective receiving cross-sections, $\langle\sigma^{\mathrm{a}}_{\mathrm{i};j}\rangle$, seen by devices at the PCB ports. This is fixed by the PCB design (to first approximation – in densely packed enclosures it will be affected by its surroundings).
2. By reducing the internal power density in the enclosure.

There are a number of ways to reduce the internal power density:

1. Reducing the external power density. However, the external environment is often uncontrolled or defined by EMC standards.
2. Reducing the total (intrinsic) transmission cross-section, $\langle\sigma^{\mathrm{t}}\rangle$, of the enclosure. This is usually limited by the necessity of providing thermal ventilation, wired connections and the capabilities of shielding technologies (e.g. gaskets, finger-stock, cable termination…) at high frequencies.
3. Increasing the absorption cross-section of the enclosure contents. This can be partly achieved using the non-susceptible contents in the enclosure, $\langle\sigma^{\mathrm{a}}_{\mathrm{i;passive}}\rangle$, and partly by *balancing* the power absorbed by the circuit loads, $\langle\sigma^{\mathrm{a}}_{\mathrm{i;circuit}}\rangle$. Addition of absorber to the inside of shielding cans is also a common remedial approach to EMC problems that are only detected at a late stage of product development.

The latter balancing effect is clearly critical since any strong coupling into a particular PCB load is a potential susceptibility problem that we are trying to avoid. Nevertheless, the average absorption of power by a PCB has a very important impact on the overall EM environment inside a densely populated enclosure and therefore on the immunity of the PCB itself and other PCBs in the equipment enclosure.

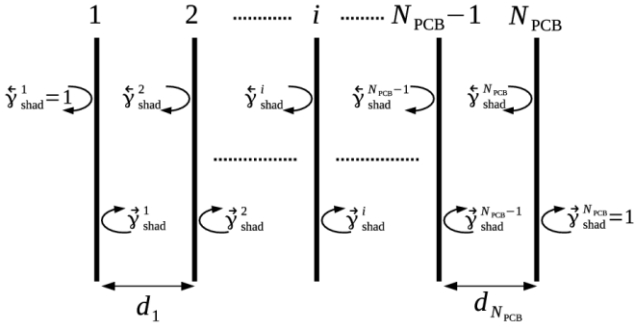

Fig. 3. Definition of shadowing factors in a stack of N_{PCB} PCBs.

D. Shadowing effects in stacked PCBs

The close proximity of the PCBs inside typical ICT enclosures will cause "shadowing effects" that reduce the ACS of the overall PCB stack compared to the sum of the individual ACSs of each PCB. We postulate that the ACS of a stack of N_{PCB} PCBs, as shown in Fig. 3, can be written as

$$\langle\sigma^{\mathrm{a}}_{\mathrm{stack}}\rangle = \frac{1}{2}\sum_{i=1}^{N_{\mathrm{PCB}}} \left(\overleftarrow{\gamma}^{i}_{\mathrm{shad}} + \vec{\gamma}^{i}_{\mathrm{shad}}\right)\langle\sigma^{\mathrm{a}}_{i}\rangle, \tag{18}$$

where $\langle\sigma^{\mathrm{a}}_{i}\rangle$ is the ACS of PCB number i in isolation and the overall shadowing factor, $0 \le \gamma_{\mathrm{shad}} \le 1$, of each PCB

$$\gamma^{i}_{\mathrm{shad}} = \frac{1}{2}\left(\overleftarrow{\gamma}^{i}_{\mathrm{shad}} + \vec{\gamma}^{i}_{\mathrm{shad}}\right), \tag{19}$$

has been divided into two parts, $\overleftarrow{\gamma}^{i}_{\mathrm{shad}}$ and $\vec{\gamma}^{i}_{\mathrm{shad}}$, for the shadowing of PCB i due to the PCBs on either side of it in the stack. The externally facing sides of the PCBs at the two ends of the stack are assumed to be un-shadowed so that $\overleftarrow{\gamma}^{1}_{\mathrm{shad}}$=$\vec{\gamma}^{N_{\mathrm{PCB}}}_{\mathrm{shad}} = 1$. Note that in general $\vec{\gamma}^{i}_{\mathrm{shad}} \neq \overleftarrow{\gamma}^{i+1}_{\mathrm{shad}}$, as can be easily appreciated by considering the case when the two PCBs are different sizes. If two PCBs, i and i+1, are similar in size and construction then it may be that $\vec{\gamma}^{i}_{\mathrm{shad}} \approx \overleftarrow{\gamma}^{i+1}_{\mathrm{shad}}$. This model can only be an approximation to reality since the shadowing may affect the nature of the field incident on each PCB and therefore the absorption efficiencies of each PCB in the stack may be different to when it is isolated.

III. Printed Circuit Boards

The absorption characteristics of a collection of 23 PCBs from two different ICT cabinets were subjected to ACS measurement in a reverberation chamber. The PCBs were fabricated using FR-4 substrates with six to twelve layers.

The PCBs' surfaces ranged from sparsely populated open tracks, to areas covered with heat-sinks and large shielding cans so the surface absorption characteristics of the PCBs are likely to vary significantly. We therefore classified the PCBs after a visual inspection according to the number of sides,

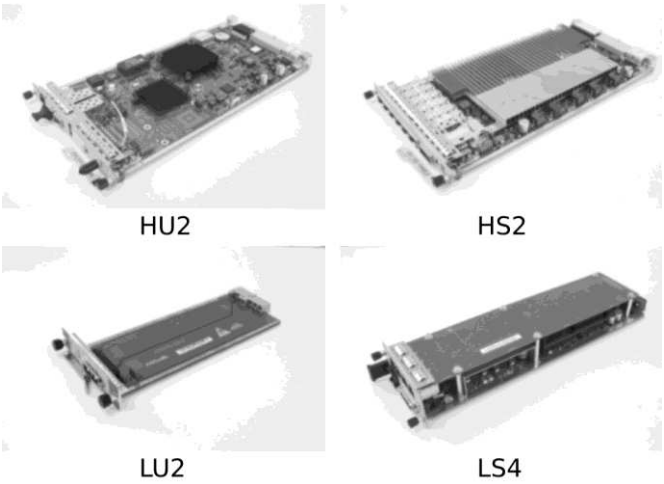

Fig. 4. Photographs of one PCB from each of the four defined classes.

TABLE II
PCB CLASSIFICATION SCHEME: <*CD*><*SS*><*n*>

Tag	Values	Interpretation
<*CD*>	L	Low component density
	H	High component density
<*SS*>	U	Low proportion of surface shielding
	S	High proportion of surface shielding
<*n*>	1	One-sided absorption (one side is ground plane)
	2	Two-sided absorption (typical case)
	4	Four-sided absorption (two PCB mini-stack)

TABLE III
CHARACTERISTICS OF THE 23 PCBS MEASURED

Length, *l* (mm)	Width, *w* (mm)	Classification	Number of PCBs
210	85	LU2	1
210	150	HU2	1
210	170	HU2	2
210	170	LU2	1
283	75	LS4	2
283	145	HU2	6*
283	145	HS2	2
365	210	HU2	8

* Four PCBs from this group were used for the stack measurements.

component density and proportion of their surface area that were shielded, either intentionally by shielding cans or as a consequence of heatsinks. The classification scheme consists of a two letter and single number "tag" as defined in Table II. The main characteristics of the PCBs, including their classifications are given in Table III. Fig. 4 shows a photograph of one PCB from each of the four classes.

The average absorption efficiency, $\langle Q^{\mathrm{a}} \rangle$, of an object is defined as the ratio of its average ACS to its average silhouette area, $\langle G \rangle$, and normalizes out the overall size of the object. For a convex object $\langle G \rangle = A_{\mathrm{S}}/4$, where A_{S} is its surface area [22]. Hence the absorption efficiency (AE) of a PCB is given by

$$\langle Q^{\mathrm{a}} \rangle = \frac{\langle \sigma^{\mathrm{a}} \rangle}{\langle G \rangle} = \frac{4}{A_{\mathrm{S}}} \langle \sigma^{\mathrm{a}} \rangle = \frac{4}{nlw} \langle \sigma^{\mathrm{a}} \rangle, \tag{20}$$

where *n* is the number of absorbing sides, *l* the length and *w* the width.

In order to quantify the shadowing of PCBs in a stack a subset of four equally sized PCBs, which formed a stack in one of the enclosures and were all of class HU2, were measured in three pairs, two sets of three and all together in the order they appeared in the enclosure. The spacing of the PCBs was 20 mm, the same as when the PCBs were installed in the enclosure, and for these initial experiments the back-planes of the PCBs were not connected together. The front of the PCBs, which were grounded to the front plates of the enclosure rail were in contact during the measurements.

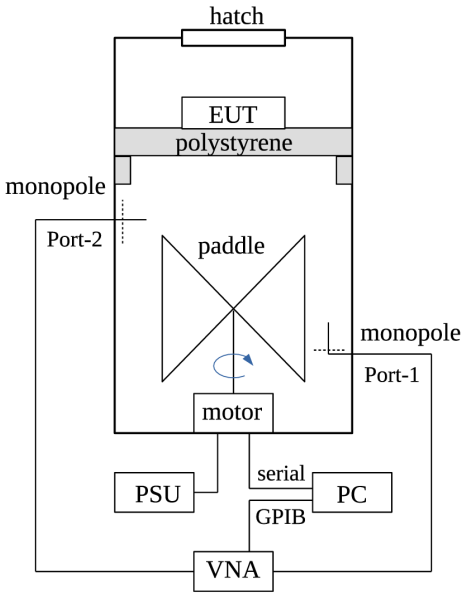

Fig. 5. Schematic illustration of RC setup for the PCB ACS measurements.

IV. MEASUREMENT METHODOLOGY

The ACS of each PCB was measured in an RC of dimensions 0.6 m × 0.7 m × 0.8 m using the methodology described in [14]. This size of chamber was necessary in order for the measurable range of ACS to cover the expected range of PCB ACSs [15]. The experimental setup is shown in Fig. 5. The chamber was tuned using a stepped mechanical paddle with 100 equal spaced angles and frequency tuning over a bandwidth of 100 MHz was also employed. The average chamber power transfer function, $\langle |S_{21}|^2 \rangle$, between two monopole antennas was measured from 2-20 GHz with a frequency resolution of 2 MHz using a vector network analyzer (VNA).

The essence of the measurement is that the ACS of an object is the difference between the total ACSs of the chamber with and without the object inside. Since the total ACS is inversely related to the chamber power transfer function the ACS of the object can be determined from [14]

$$\langle \sigma^{\mathrm{a}}_{\mathrm{PCB}} \rangle = \frac{\lambda^2}{8\pi} \eta_1^{\mathrm{T}} \eta_2^{\mathrm{T}} \left(\frac{1}{\langle |S_{21}^{\mathrm{loaded}}|^2 \rangle} - \frac{1}{\langle |S_{21}^{\mathrm{unloaded}}|^2 \rangle} \right), \tag{21}$$

where λ is the wavelength, η_i^{T} are the total radiation efficiencies of the two antennas and $\langle |S_{21}^{\mathrm{loaded}}|^2 \rangle$ and $\langle |S_{21}^{\mathrm{unloaded}}|^2 \rangle$ are the loaded and unloaded chamber power transfer functions respectively. The total radiation efficiencies are given by the products of the dissipative radiation efficiencies due to ohmic and dielectric losses on the antennas

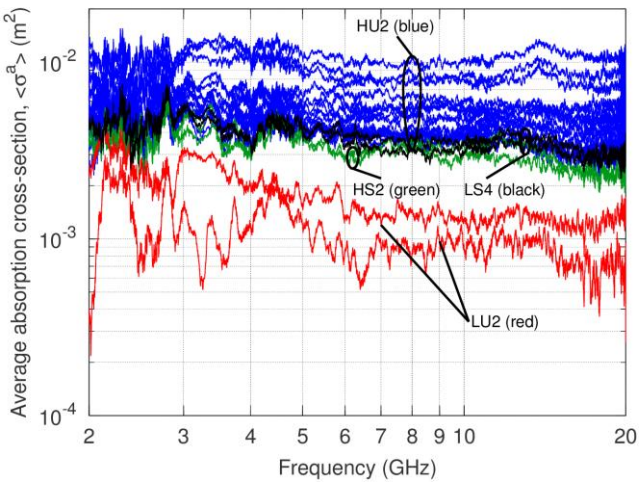

Fig. 6. The measured ACS of all the PCBs identifying those in each class.

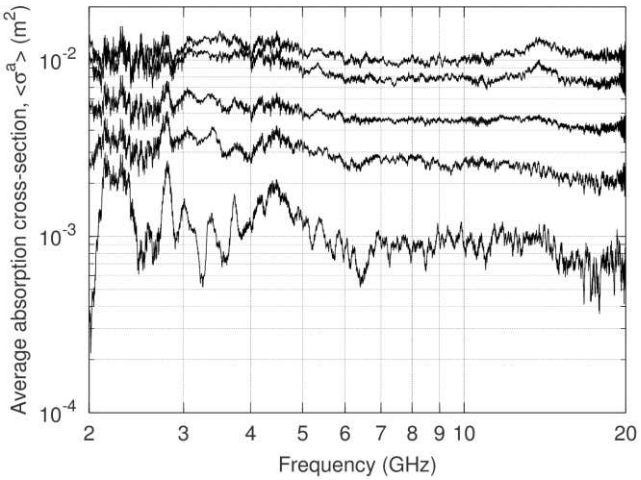

Fig. 7. Quantiles of the measured ACS of the PCBs. From top to bottom the maximum, 90th percentile, median, 10th percentile and minimum are shown.

(η_i^{rad}) and the reflection mismatch factors $\left(1-\left|S_{ii}^{\mathrm{FS}}\right|^2\right)$ of each antenna, where S_{ii}^{FS} denotes the free-space reflection coefficient of the antennas.

The overall measurement procedure was validated using a collection of objects with known ACS [15]. The uncertainty in the ACS is estimated to be ±15 %.

V. Results

The measured ACSs of all the PCBs are shown in Fig. 6, identifying those in each class. Overall the ACS ranges from 4×10^{-4} m^2 to just over 10^{-2} m^2 and has a generally decreasing trend with frequency. The HU2 and HS2 class PCBs are mixed together in the main cluster of graphs between 2×10^{-3} m^2 and 10^{-2} m^2 with no discernible distinction between the two classes. The LS4 class PCBs are both located on the lower edge of this main group with ACSs in the range 3×10^{-3} m^2 to 5×10^{-3} m^2. The LU2 PCBs form a distinct group with much lower ACSs in the range 6×10^{-4} m^2 to 2×10^{-3} m^2. These PCBs also show greater variation with frequency, particularly at lower frequencies when they also have a greater difference between themselves. Note that the measurement

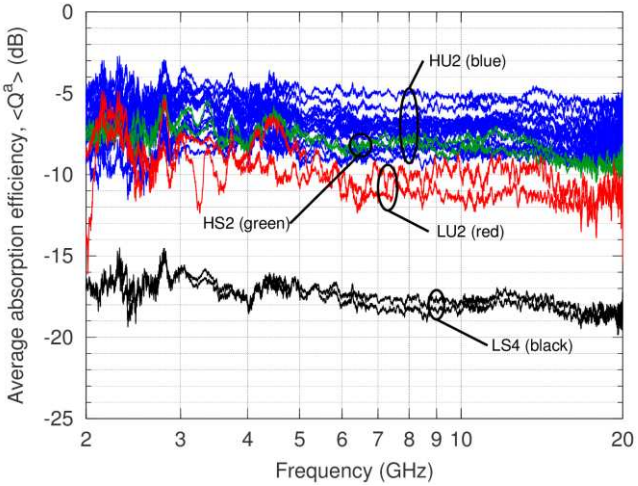

Fig. 8. The measured AE of all the PCBs identifying those in each class.

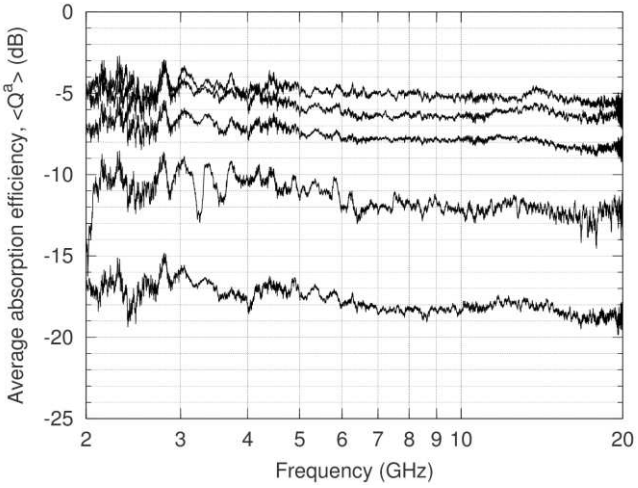

Fig. 9. Quantiles of the measured AE of the PCBs. From top to bottom the maximum, 90th percentile, median, 10th percentile and minimum are shown.

uncertainty is greater in the low frequency band, particularly from 2-3 GHz, due to a lower number of independent field samples and larger amount of non-stochastic energy in the chamber [15].

The quantiles of the measured ACSs are shown in Fig. 7. The median ACS is relatively flat, falling from 6×10^{-3} m^2 at 2 GHz to 4×10^{-3} m^2 at 20 GHz. The 10-th and 90-th percentiles range between 2×10^{-3} m^2 and about 10^{-2} m^2.

Using (20) and the characteristics in Table III the AE of each PCB was determined. Fig. 8 shows the results for all the PCBs. The bulk of the PCBs have AEs in the range -12 dB to -5 dB. There is a slightly decreasing trend in the AE with frequency for most of the PCBs. Again there was no significant distinction between the HU2 and HS2 class PCBs. The LU2 PCBs had AEs located at the bottom of the main group, becoming distinctly separated from the main group above 6 GHz. The LS4 PCBs had much lower AE than all the others, ranging from -20 dB to -16 dB. Since these PCBs were "mini-stacks" of two PCBs with four sides, according to our definition in Table III, this suggested strong shadowing of the two facing sides in the mini-stack. Put another way, in terms of absorption the mini-stacks appear to behave more like two-

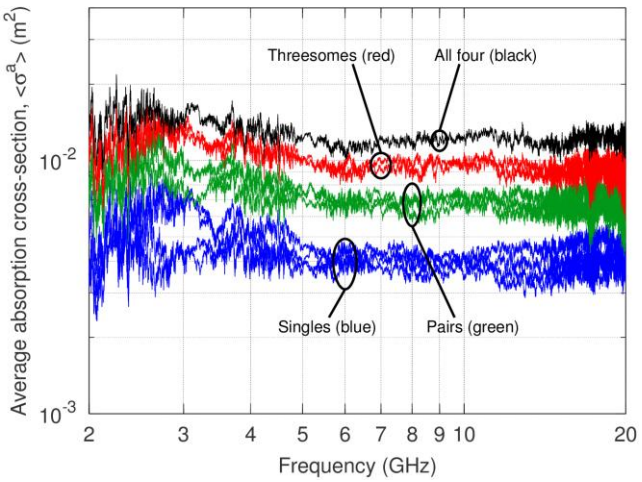

Fig. 10. The measured ACS of various sub-stacks of four HU2 class PCBs.

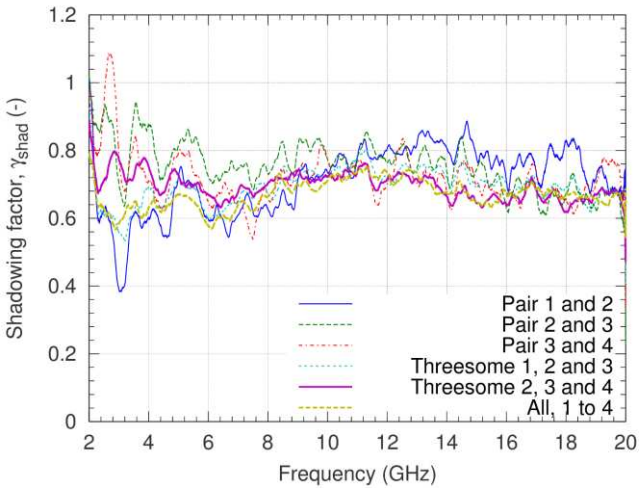

Fig. 11. Estimated shadowing factor of the four HU2 PCBs, assuming that it is the same for all sides of each PCB.

TABLE IV
SUMMARY STATISTICS OF THE MEASURED PCB ACSS, $\langle\sigma^a\rangle$, AND ABSORPTION EFFICIENCIES, $\langle Q^a\rangle$, IN DIFFERENT FREQUENCY BANDS. HERE E[·] DENOTES THE EXPECTATION VALUE, VAR[·] THE VARIANCE AND COV[·] THE COEFFICIENT OF VARIATION.

Statistic	3 GHz	6 GHz	10 GHz	15 GHz	20 GHz
$\mathrm{E}[\langle\sigma^a\rangle]$ (cm^2)	61	47	46	43	41
$\sqrt{\mathrm{Var}[\langle\sigma^a\rangle]}$ (cm^2)	25	21	21	24	23
$\mathrm{CoV}[\langle\sigma^a\rangle]$ (-)	0.40	0.45	0.46	0.56	0.55
$\mathrm{E}[\langle Q^a\rangle]$ (-)	0.22	0.17	0.17	0.15	0.15
$\sqrt{\mathrm{Var}[\langle Q^a\rangle]}$ (-)	0.09	0.07	0.07	0.07	0.07
$\mathrm{CoV}[\langle Q^a\rangle]$ (-)	0.43	0.43	0.41	0.45	0.44

sided PCBs. The quantiles of the AE are shown in Fig. 9. The median AE is -10 dB at 2 GHz, falling gradually to -12 dB at 20 GHz. The 10-th and 90-th percentiles span the range -12 dB to -6 dB. Due to the nature of the LS4 class PCBs the separation between the minimum and 10-th percentile AE is much greater than that between the 90-th percentile and maximum AE.

Table IV provides a summary of the main statistics of the measured PCB ACSs and derived AEs, giving the expectation value, standard deviation and coefficient of variation of each in five frequency bands.

The ACSs of the PCB stacks are shown in Fig. 10. It can be seen that the ACSs of all the single PCBs, pairs and threesomes are well separated into groups with relatively little variation within the groups. The ACSs are not exactly additive, indicating that shadowing between the PCBs is a significant effect. Since all four of the PCBs investigated in the stack measurements were the same size and there is little apparent difference in the ACS of the different pairs and threesome we assumed that the shadowing factor of all the PCB faces (except for those on the ends of the stack which were taken to be unity) are the same. Using this assumption and (18) specialized to each stack the shadowing factor can be estimated from each measurement. The results are shown in Fig. 11. The shadowing factors from the different measurements are quite consistent and above 4 GHz are mostly within the range 0.6 to 0.8, indicating that 20% - 40 % less power is absorbed by the faces of the PCBs inside the stacks compared to when the PCBs are isolated. There is an overall trend to a maximum in the shadowing factor at 12-14 GHz. Below about 5 GHz, there is more variability in the shadowing factors suggesting that specific features of the PCBs may be playing more of a role.

VI. CONCLUSIONS

Determining the shielding effectiveness of an enclosure under real operating conditions is of great importance in ensuring the electromagnetic compatibility of the systems it contains. The shielding effectiveness of the enclosure depends directly on the energy absorbed by its contents. In this paper a comprehensive data-set for the average ACS of modern ICT PCBs has been measured using a reverberation chamber. The acquired data is directly applicable to the high–frequency power balance analysis of shielding by electrically large equipment enclosures and the development of future electromagnetic compatibility qualification methodologies for enclosures and PCBs. In particular the results and the methodology used to obtain them provide a basis for extending earlier work on the use of “representative contents” in the characterization of enclosure shielding, as described in Annex K of IEEE 299.1, to the higher frequencies necessitated by current trends in ICT. Using a review of the power balance analysis of both the immunity and emissions perspectives of a populated enclosure we demonstrated how the average ACS of the contents impacts on the overall shielding effectiveness of the enclosure.

We were able to classify the PCBs according to their external physical attributes and derived their average absorption efficiencies, which provide a PCB size independent measure of the absorption. While average ACS is essentially a far-field quantity we were able to empirically quantify the “shadowing effect” when the PCBs were stacked together in close proximity to each other as they typically are in modern ICT enclosures. Here we have assumed the PCBs are located more than a quarter-wavelength from the enclosure walls; further work is necessary to investigate the effect on the

absorption of bringing the enclosure walls much closer to the PCB stack and if average ACS remains a useful metric in this case.

REFERENCES

[1] J. F. Dawson, J. Ahmadi and A. C. Marvin, "Reduction of radiated emissions from apertures in resonant enclosures by the use of absorptive materials," *8th International Conference on Electromagnetic Compatibility*, Edinburgh, U.K., pp. 207-212, 21-24 September 1992.

[2] N. Izzat, G. H. Hilton, C. J. Railton and S. Meade, "Use of resistive sheets in damping cavity resonance", *Electronics Letters*, vol. 32, no. 8, pp. 721-722, April 1996.

[3] A. C. Marvin, J. F. Dawson, S. Ward, L. Dawson, J. Clegg and A. Weissenfeld, "A proposed new definition and measurement of the shielding effect of equipment enclosures", *IEEE Transactions on Electromagnetic Compatibility*, vol. 46, no. 3, pp. 459–468, 2004.

[4] A. C. Marvin and Y. Cui, "Towards evaluating the shielding of enclosures with contents at frequencies above 1 GHz", *IEEE International Symposium on Electromagnetic Compatibility*, Chicago, IL, pp. 200–205, 8-12 August, 2005.

[5] IEEE-STD 299.1, "Standard method for measuring the shielding effectiveness of enclosures and boxes having all dimensions between 0.1 m and 2 m", *Institute of Electrical and Electronics Engineers*, Piscataway, NJ, October 2013.

[6] A. Gifuni, "Relation between the shielding effectiveness of an electrically large enclosure and the wall material under uniform and isotropic field conditions", *IEEE Transactions on Electromagnetic Compatibility*, vol. 55, no. 6, pp. 1354-1357, December 2013.

[7] L. J. Washbourne, V. Rajamani, C. F. Bunting, J. C. West, B. Archambeault and S. Connor, "Effectiveness of absorbing materials on reducing electromagnetic emissions from cavities measured using a nested reverberation chamber approach", *IEEE International Symposium on Electromagnetic Compatibility*, Raleigh, NC, pp. 909-912, 4-8 August 2014.

[8] W. Wallyn and D. De Zutter, "Modeling the shielding effectiveness and resonances of metallic shielding enclosures loaded with PCBs", *IEEE International Symposium on Electromagnetic Compatibility*, Montreal, Canada, pp. 691–696, 13-17 August, 2001.

[9] D. W. P. Thomas, A. Denton, T. Konefal, T. M. Benson, C. Christopoulos, J. F. Dawson, A. C. Marvin and S. J. Porter, "Characterisation of the shielding effectiveness of loaded equipment enclosures", *International Conference and Exhibition on Electromagnetic Compatibility (EMC York 99)*, York, UK, pp. 89–94, 12-13 July, 1999.

[10] D. Jing and H. Guo, "Study on coupling characteristics for EM pulse into slotted shell of loaded PCB", *International Conference on Computer, Mechatronics, Control and Electronic Engineering (CMCE),* Changchun, China, pp. 398–401, 24-26 August, 2010.

[11] S. Yenikaya, "Hybrid MoM/FEM modelling of shielding effectiveness of loaded rectangular enclosures with apertures", *IEEE International Symposium on Electromagnetic Compatibility,* Austin, TX, pp. 61–65, 17-21August, 2009.

[12] M. P. Robinson, S. J. Porter and P. O. Oorth, "Reflection and transmission coefficients of printed circuit boards", *4th European Symposium on Electromagnetic Compatibility,* Brugge, vol. 2 pp. 209-213, 11-15 September, 2000.

[13] A. Lozano, M. P. Robinson, A. Díaz and J. V. Balbastre, "Evaluation and optimization of an equivalent model for printed circuit boards inside metallic enclosures", *Proceedings of the XXIX General Assembly of the International Union of Radio Science (URSI)*, Chicago, IL, Paper Number EBp6, 7-16 August, 2008.

[14] U. Carlberg, P.-S. Kildal, A. Wolfgang, O. Sotoudeh, and C. Orlenius, "Calculated and measured absorption cross sections of lossy objects in reverberation chamber", *IEEE Transactions on Electromagnetic Compatibility*, vol. 46, no. 2, pp. 146–154, May 2004.

[15] I. D. Flintoft, S. J. Bale, S. L. Parker, A. C. Marvin, J. F. Dawson and M. P. Robinson, "On the measureable range of absorption cross-section in a reverberation chamber", *IEEE Transactions on Electromagnetic Compatibility*, accepted for publication Nov. 2015. DOI: 10.1109/TEMC.2015.2499841.

[16] A. Gifuni, "On the measurement of the absorption cross section and material reflectivity in a reverberation chamber", *IEEE Transactions on Electromagnetic Compatibility*, vol. 51, no. 4, pp. 1047-1050, 2009.

[17] A. Gifuni, A. Sorrentino, A. Fanti, G. Ferrara, M. Migliaccio, G. Mazzarella and F. Corona, "On the evaluation of the shielding effectiveness of an electrically large enclosure", *Advanced Electromagnetics*, vol. 1, no. 1, pp. 84-91, May 2012.

[18] D. A. Hill, M. T. Ma, A. R. Ondrejka, B. F. Riddle, M. L. Crawford and R. T. Johnk, "Aperture excitation of electrically large, lossy cavities", *IEEE Transactions on Electromagnetic Compatibility*, vol. 36, no. 3, pp. 169-178, August 1994.

[19] I. Junqua, J.-P. Parmantier and F. Issac, "A network formulation of the power balance method for high-frequency coupling", *Electromagnetics*, vol. 25, no. 7-8, pp. 603-622, 2005.

[20] P. F. Wilson, D. A. Hill and C. L. Holloway, "On determining the maximum emissions from electrically large sources", *IEEE Transactions on Electromagnetic Compatibility*, vol. 44, no. 1, pp. 79-86, 2002.

[21] A. C. Marvin and Y. Cui, "Shielding measurements of equipment enclosures in the radiating near field", *IEEE Transactions on Electromagnetic Compatibility*, vol. 49, no. 4, pp. 860–867, 2007.

[22] V. Vouk, "Projected area of convex bodies", *Nature*, vol. 162, pp. 330-331, August 1948.